


Acoustic anti-parity-time symmetric structure enabling equivalent lasing and coherent perfect absorption

Ting Hu , Qi Wei *, Xing-Feng Zhu , Jie Yao , and Da-Jian Wu [†]
*Jiangsu Key Laboratory of Opto-Electronic Technology, School of Physics and Technology,
 Nanjing Normal University, Nanjing 210023, China*

 (Received 10 June 2021; revised 12 September 2021; accepted 13 October 2021; published 27 October 2021)

Non-Hermitian systems with parity-time (\mathcal{PT}) symmetry have attracted increasing interest due to their intriguing properties and associated applications. Inspired by that, we propose here an acoustic anti-parity-time ($A\text{-}\mathcal{PT}$) symmetric structure with metamaterials featuring balanced positive and negative indices, together with equal gain/loss. According to the derived scattering matrix, we demonstrate its extraordinary scattering properties. For example, the spontaneous phase transition of the scattering matrix is observed, by simply modulating the frequency, gain/loss, or geometric width. In the absence of gain/loss, the $A\text{-}\mathcal{PT}$ symmetric structure degrades into a pair of complementary media, resulting in bidirectional total transmission. At the zero and pole of the scattering matrix, the structure behaves as an acoustic coherent perfect absorber and equivalent laser, respectively, which can perfectly absorb two-port coherent incident waves and radiate two coherent output waves with extensive and equal amplitudes. Different from that in the \mathcal{PT} symmetric structure, these three effects based on the $A\text{-}\mathcal{PT}$ symmetric structure are all achieved in the symmetric phase of the scattering matrix, resulting in the symmetric intensity distributions. Besides, the coherent perfect absorption and lasing modes of the $A\text{-}\mathcal{PT}$ symmetric structure are continuous and symmetric in the parameter space, which may facilitate further experimental realizations. The proposed $A\text{-}\mathcal{PT}$ symmetric structure provides an alternative method to demonstrate the physics of the non-Hermitian Hamiltonian, and may offer an alternative approach to design acoustic functional devices such as absorbers, sensors, and amplifiers.

DOI: [10.1103/PhysRevB.104.134110](https://doi.org/10.1103/PhysRevB.104.134110)

I. INTRODUCTION

Recently, non-Hermitian systems, such as the famous parity-time (\mathcal{PT}) symmetric structure, have attracted increasing interest due to their intriguing properties and associated applications. In 1998, Bender and Boettcher proved that non-Hermitian Hamiltonian with \mathcal{PT} symmetry, defined by $[\mathcal{PT}, H] = 0$, could have a real energy spectrum up to a critical value of the imaginary part of the potential parameter [1]. At the critical value, which is referred to later as an exceptional point, the \mathcal{PT} symmetry will be broken spontaneously, resulting in a spontaneous phase transition from symmetric phase to symmetry-broken phase, where the spectrum becomes complex. The concept of \mathcal{PT} symmetry was further introduced into the fields of optics and acoustics based on the analogy between the Schrödinger equation in quantum mechanics and the classical wave equation [2–18]. \mathcal{PT} symmetric systems, which were realized based on balanced gain and loss [2–13] or loss alone [14–18], exhibited numerous interesting and unusual phenomena, such as power oscillations [2–4], simultaneous coherent perfect absorption (CPA) and lasing [5–8], anisotropic transmission resonances [9], topological states [10,16], one-way cloaking [11], invisible

sensing [12], phonon lasing [13], optical transparency [14], asymmetric transport [15], and unidirectional focusing [17].

As another striking non-Hermitian Hamiltonian, anti-parity-time ($A\text{-}\mathcal{PT}$) symmetry, defined by $\{\mathcal{PT}, H\} = 0$, may facilitate the experiments since it requires either gain or loss [19–28]. $A\text{-}\mathcal{PT}$ symmetric systems were proposed based on positive and negative index materials [19], cold-atom lattices [20], flying atoms [21], nonlinear structure [22], coupled waveguide systems [23–25], electrical circuit resonators [26], and opposite convection flows [27]. Such systems lead to various intriguing effects, such as continuous lasing spectrum [19], constant refraction [23], chiral mode conversion [24], energy difference conserving dynamics [26], and coherent switch [28]. However, there have not been many reports of acoustic $A\text{-}\mathcal{PT}$ symmetric structure. On the other hand, metamaterials have been widely demonstrated to control acoustic waves, but previous efforts were mostly based on modulating the real parts of the constitutive parameters [29–49]. The acoustic $A\text{-}\mathcal{PT}$ symmetric structure, if it is realized based on metamaterials, may extend the study of metamaterials into the realm of complex constitutive parameters.

In this paper, we propose a one-dimensional (1D) acoustic $A\text{-}\mathcal{PT}$ symmetric structure with metamaterials, which features balanced positive and negative indices, together with equal gain/loss, namely, a complex refractive index satisfying $n(x) = -n^*(-x)$. The transfer matrix method is employed to derive the acoustic propagation and scattering matrix of the $A\text{-}\mathcal{PT}$ symmetric structure. By modulating the structure

*weiqi@njnu.edu.cn

[†]wudajian@njnu.edu.cn

respectively, as (see Appendix A)

$$\begin{aligned}
M_{1,1} &= \frac{1}{4(\alpha^2 + \delta^2)} [4\delta^2 \cos \gamma - 2\delta(-\alpha^2 - \delta^2 + 1) \sin \gamma + \alpha(\alpha^2 + \delta^2 + 2\alpha + 1)e^\chi + \alpha(-\alpha^2 - \delta^2 + 2\alpha - 1)e^{-\chi}], \\
M_{1,2} &= \frac{1}{4(\alpha^2 + \delta^2)} [4i\alpha\delta \cos \gamma - 2\delta(-\alpha^2 - \delta^2 - 1) \sin \gamma + \alpha(\alpha^2 + \delta^2 - 2i\delta - 1)e^\chi + \alpha(-\alpha^2 - \delta^2 - 2i\delta + 1)e^{-\chi}], \\
M_{2,1} &= \frac{1}{4(\alpha^2 + \delta^2)} [4i\alpha\delta \cos \gamma - 2\delta(\alpha^2 + \delta^2 + 1) \sin \gamma + \alpha(-\alpha^2 - \delta^2 - 2i\delta + 1)e^\chi + \alpha(\alpha^2 + \delta^2 - 2i\delta - 1)e^{-\chi}], \\
M_{2,2} &= \frac{1}{4(\alpha^2 + \delta^2)} [4\delta^2 \cos \gamma - 2\delta(\alpha^2 + \delta^2 - 1) \sin \gamma + \alpha(-\alpha^2 - \delta^2 + 2\alpha - 1)e^\chi + \alpha(\alpha^2 + \delta^2 + 2\alpha + 1)e^{-\chi}]. \quad (3)
\end{aligned}$$

Here, $\chi = 2\delta k_0 d$ and $\gamma = 2\alpha k_0 d$. It is straightforward to find that

$$\text{Im}(M_{1,1}) = \text{Im}(M_{2,2}) = 0, \quad M_{1,2} = -M_{2,1}^*, \quad \det(M) = 1. \quad (4)$$

It is worth pointing out that the equation $\det(M) = 1$ originates from reciprocity [53], which can be proved as follows. For the case of single left (labeled L) or right (labeled R) incidence, where the respective boundary condition $B = 0$ or $C = 0$ is imposed, the complex transmission (t_L or t_R) and reflection (r_L or r_R) coefficients of the A- \mathcal{PT} symmetric structure can be expressed in terms of the components of the transfer matrix M as

$$\begin{aligned}
t_L &= \frac{M_{1,1}M_{2,2} - M_{1,2}M_{2,1}}{M_{2,2}}, \quad t_R = \frac{1}{M_{2,2}}, \\
r_L &= \frac{M_{1,2}}{M_{2,2}}, \quad r_R = -\frac{M_{2,1}}{M_{2,2}}. \quad (5)
\end{aligned}$$

Acoustic reciprocity holds for the proposed system, since there is no nonlinearity, moving media, spatiotemporal modulation, and bianisotropy [54]. Reciprocity guarantees symmetrical relations between field quantities when sources and receivers are interchanged. For the proposed system, therefore, acoustic reciprocity straightforwardly leads to $t_L = t_R$. By inserting Eq. (5) into $t_L = t_R$, one can finally obtain $M_{1,1}M_{2,2} - M_{1,2}M_{2,1} = 1$, namely, $\det(M) = 1$.

Equation (5), together with acoustic reciprocity, states that the acoustic transmissions of the A- \mathcal{PT} symmetric structure under left and right incidence are always equal, independent of the incident direction. Hereafter, they are uniformly denoted as $t = t_L = t_R = 1/M_{2,2}$. However, the reflections for left and right incidence are different from each other in general. By inserting Eq. (3) into Eq. (5), the transmission and reflections can then be explicitly expressed. Equations (4) and (5) can further lead to

$$\text{Im}(t) = 0, \quad r_L = r_R^*, \quad (6)$$

which are nothing else but the intrinsic properties of a 1D A- \mathcal{PT} symmetric structure (see Appendix B). For the case of one-port incidence, the pure real-valued t indicates that the transmitted wave is either in phase or antiphase with the incident wave, while $r_L = r_R^*$ states that the left and right reflections are equal in amplitude but with opposite phase. Namely, the left reflectance ($R_L = |r_L|^2$) and right reflectance ($R_R = |r_R|^2$) are equal, so they are uniformly denoted as the

reflectance:

$$R = R_L = R_R = |r_{L(R)}|^2. \quad (7)$$

It is different for the \mathcal{PT} symmetric structure, where the amplitudes of the left and right reflections are usually unequal and their phase difference is 0 or π , and the transmission coefficient is usually complex [5–8].

Based on the transmission (t) and reflections (r_L and r_R), the scattering matrix S of the A- \mathcal{PT} symmetric structure, which relates the two outgoing waves and the two incoming waves through $\begin{bmatrix} A \\ B \end{bmatrix} = S \begin{bmatrix} C \\ D \end{bmatrix}$, can be further deduced as

$$S = \begin{bmatrix} r_L & t \\ t & r_R \end{bmatrix}. \quad (8)$$

IV. SCATTERING PROPERTIES

Equation (5) states that the transmission and reflections are dependent on the variables d , δ , and the circular frequency (ω) of the acoustic wave. Therefore, there are three approaches to adjusting the scattering properties: tailoring the gain/loss of the materials, tuning the frequency of the incident acoustic wave, and scaling the structure geometric size. The third approach is more practical because the first two approaches suffer from the material dispersion. In this paper, we mainly discuss the effect of the variation of these three parameters on the scattering characteristics of the A- \mathcal{PT} symmetric structure. To verify the validity of the analytical results, numerical simulations based on the finite element method are also carried out to demonstrate the pressure field distributions of the system. The height of the structure does not influence the acoustic scattering, and it is set to 2 m in all numerical simulations.

A. Spontaneous phase transition of the scattering matrix

The scattering matrix described by Eq. (8) has two eigenvalues as

$$\lambda_{\pm} = \text{Re}(r_L) \pm \sqrt{t^2 - \text{Im}^2(r_L)}, \quad (9)$$

and the corresponding two eigenvectors are

$$\Psi_{\pm} = \begin{bmatrix} B_{\pm} \\ C_{\pm} \end{bmatrix} = \begin{bmatrix} -t \\ i\text{Im}(r_L) \mp \sqrt{t^2 - \text{Im}^2(r_L)} \end{bmatrix}. \quad (10)$$

Each eigenvector of the S matrix corresponds to a scattering eigenstate, where two particular coherent waves with amplitudes of B_+ (or B_-) and C_+ (or C_-) are simultaneously incident on the structure from the left and right sides, respectively, and the amplitudes of the two scattered waves are λ_+B_+ (or λ_-B_-) and λ_+C_+ (or λ_-C_-) [9]. For a scattering eigenstate, the corresponding eigenvalue quantitatively describes how the incident waves are scattered, since the ratio between the amplitudes of the scattered and incident waves is $|\lambda_{\pm}|$. Therefore, $|\lambda_{\pm}|$ could be referred to as the scattering strengths for the eigenstates.

Equations (9) and (10) suggest two phases for both the eigenvalues and eigenvectors of the scattering matrix, which correspond to two different scattering behaviors. When $|t| > |\text{Im}(r_L)|$, each eigenvector is \mathcal{PT} symmetric itself, i.e., $PT\Psi_{\pm} \propto \Psi_{\pm}$, so the eigenstates are in the \mathcal{PT} symmetric scattering phase. Besides, the intensities of the two incidences in a scattering eigenstate are equal, namely, $|B_{\pm}/C_{\pm}| = 1$. In this phase, the eigenvalues λ_{\pm} are both real but unequal (bifurcate). Real eigenvalues indicate that the two symmetric incidences are either damped or amplified without any phase added during the scattering process of an eigenstate. Moreover, unequal eigenvalues indicate that the incidences are damped/amplified with different strengths for the two eigenstates. The other phase, where $|t| < |\text{Im}(r_L)|$, is then referred to as the \mathcal{PT} symmetry-broken phase, since $PT\Psi_{\pm} \propto \Psi_{\mp}$, i.e., the \mathcal{PT} operation transforms one eigenvector into the other. Here, the intensities of the two incidences in a scattering eigenstate are different, namely, $|B_+/C_+| = |C_-/B_-| \neq 1$, and the eigenvalues λ_{\pm} are complex and conjugated ($\lambda_+ = \lambda_-^*$). In the symmetry-broken phase, the scattering strengths $|\lambda_{\pm}|$ are equal due to the conjugated relation of the eigenvalues, so the incidences are damped/amplified with the same strength for the two eigenstates. During the scattering process of an eigenstate in this phase, the two asymmetric incidences are scattered with an additional phase $\arg(\lambda_{\pm})$. At $|t| = |\text{Im}(r_L)|$, which is referred to as an exceptional point, a spontaneous phase transition occurs for both the eigenvalues and eigenvectors of the scattering matrix. Phase transition for eigenstates is also observed in other $A\text{-}\mathcal{PT}$ symmetric systems [23,24].

As an example, we suppose a structure with parameters $\alpha = 1.243$ and $\delta = 0.0932$ (corresponding to gain), and adjust the product of circular frequency and geometric width (ωd) to explore the spontaneous phase transition process. Figures 2(a) and 2(c) show the resulting scattering strengths $|\lambda_{\pm}|$ and $|B_{\pm}/C_{\pm}|$ versus ωd . When $\omega d < 6160$, $|\lambda_{\pm}|$ are different and $|B_{\pm}/C_{\pm}|$ are unitary, implying that the scattering matrix is in the symmetric phase. However, when $\omega d > 6160$, $|\lambda_{\pm}|$ are the same and $|B_{\pm}/C_{\pm}|$ are nonunitary, indicating that the scattering matrix is under the symmetry-broken phase. The spontaneous phase transition occurs at the exceptional point $\omega d = 6160$, where the absolute values of the eigenvalues meet and bifurcate. It can be observed that there are two sharp peaks (at $\omega d = 4080$) for the curves of $|\lambda_{\pm}|$, where two eigenvalues both tend to infinity, corresponding to the acoustic equivalent lasing mode. In this case, the point $\omega d = 4080$ is called the pole of the scattering matrix.

As another example, we only flip the sign of δ while keeping other structure parameters constant. Namely, $\alpha = 1.243$

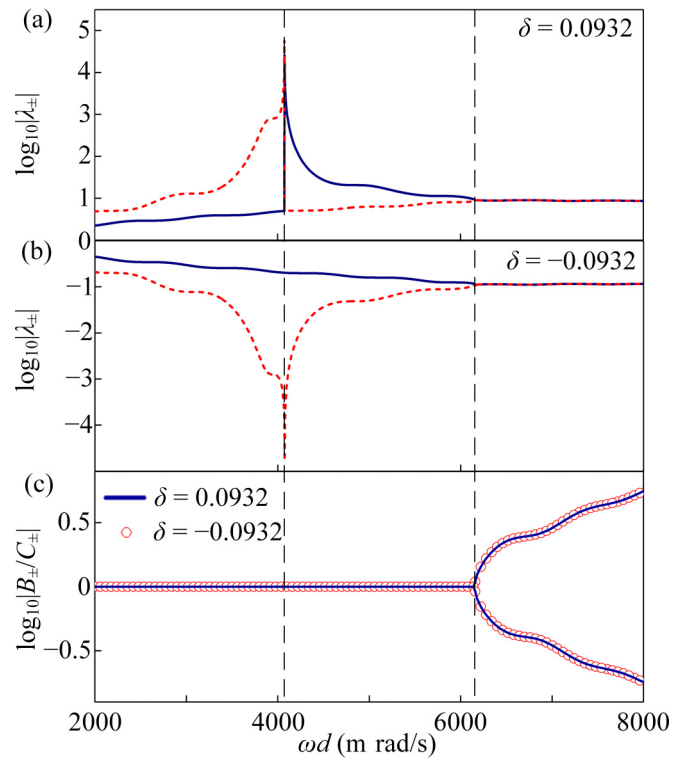


FIG. 2. Analytical results of (a), (b) the eigenvalues and (c) $|B_{\pm}/C_{\pm}|$ versus ωd . The blue solid (red dotted) line shows $|\lambda_-|$ ($|\lambda_+|$). Here, $\alpha = 1.243$ in all cases. In (a), (b), $\delta = 0.0932$ and $\delta = -0.0932$, respectively. The vertical dashed lines indicate the locations of $\omega d = 4080$ and $\omega d = 6160$, corresponding to the pole/zero and exceptional point, respectively.

and $\delta = -0.0932$ (corresponding to loss). Figures 2(b) and 2(c) show the resulting scattering strengths $|\lambda_{\pm}|$ and $|B_{\pm}/C_{\pm}|$ versus ωd . The phase transition between the symmetric phase and the symmetry-broken phase can also be observed at $\omega d = 6160$. Case $\omega d < 6160$ corresponds to the symmetric phase, while case $\omega d > 6160$ corresponds to the symmetry-broken phase. Therefore, the spontaneous phase transition process for $\delta = -0.0932$ [see Figs. 2(b) and 2(c)] is the same as that for $\delta = 0.0932$ [see Figs. 2(a) and 2(c)], and the exceptional points are both at $\omega d = 6160$. As shown in Fig. 2(c), the ratios $|B_{\pm}/C_{\pm}|$ for $\delta = \pm 0.0932$ are the same, because the ratios $|B_{\pm}/C_{\pm}|$, according to Eq. (10), are dependent on $|\delta|$. However, there is a valley, instead of the peaks for $\delta = 0.0932$, for the scattering strength curves at $\omega d = 4080$, corresponding to an acoustic CPA mode. In this case, the point $\omega d = 4080$ is called the zero of the scattering matrix.

We further explore the phase transition process of the scattering matrix in the ωd - δ parameter space, as shown in Fig. 3(a). The white region corresponds to the symmetric scattering phase, while the gray regions correspond to the symmetry-broken phase. The boundaries between the white and gray regions indicate the phase transition. When the gain/loss δ is small and the frequency is low, the scattering matrix is in the symmetric phase. When the gain/loss δ is large and the frequency is high, the scattering matrix is in the symmetry-broken phase. Therefore, for a fixed frequency, larger gain/loss always leads to the symmetry-broken phase.

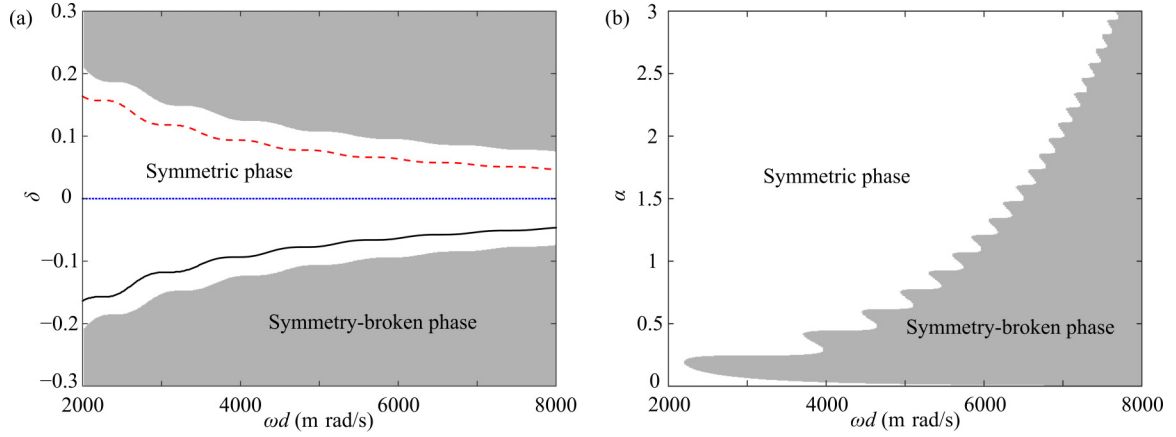


FIG. 3. Phase diagram of the scattering matrix. The blue dotted line, black solid line, and red dotted line represent the bidirectional total transmission, CPA mode, and lasing mode solutions for the A - \mathcal{PT} symmetric structure, respectively. In (a), $\alpha = 1.243$; in (b), $\delta = 0.0932$.

For a fixed gain/loss, higher frequency favors the symmetry-broken phase. Moreover, it is interesting to find out that the phase diagram of the scattering matrix is symmetric to $\delta = 0$. In the formula, this symmetric behavior originates from the phase transition being determined by the quantitative relationship between $|t|$ and $|\text{Im}(r_L)|$, which is further determined by $|\delta|$. In physics, if we flip the sign of δ , namely, replace the local gain with loss (and vice versa), and keep other structure parameters constant, the system undergoes nothing else but a time reversal. Therefore, the phase of the scattering matrix remains unchanged. Figure 3(b) depicts the phase diagram in the ωd - α parameter space. The phase boundary features a sawtooth profile. Roughly speaking, increasing α shifts the phase boundary toward high frequency. At a fixed ωd , the symmetry-broken phase lies in the range of smaller α , while the symmetric phase lies in the range of larger α .

The amplitudes and phases of the transmission and reflection are also investigated based on Eqs. (3) and (5). The model parameters are the same as that in Fig. 2(a); namely, $\alpha = 1.243$ and $\delta = 0.0932$. Figures 4(a) and 4(b) plot the transmittance ($T = |t|^2$) and reflectance R in logarithm versus ωd , where a sharp peak located at the pole (namely, $\omega d = 4080$) can be observed for both T and R . The peaks are all located at $\omega d = 4080$ for the curves of eigenvalues, transmittance, and reflectance, as shown in Figs. 2(a), 4(a), and 4(b), respectively. At the phase transition point (at $\omega d = 6160$), no particular property is found for T and R . Figures 4(c) and 4(d) show the phases of the left/right reflection and transmission coefficients versus ωd . At the pole, there is a π jump in phase for all reflection and transmission coefficients. Due to the abrupt change of phase, the delay times for all reflection and transmission coefficients show a delta function behavior as the variable ωd is varied. Therefore, at the pole, the reflected and transmitted waves can be trapped for a long time and get amplified extremely by the local gain of the structure, finally resulting in the acoustic equivalent lasing, where the transmittance and reflectance both tend to infinity, as shown in Figs. 4(a) and 4(b). Besides, the phases of two reflections are opposite to each other, and the phase of transmission is either 0 or π .

B. Bidirectional total transmission

Local gain/loss is important in an A - \mathcal{PT} symmetric structure containing PIM and NIM. There is a special case where the local gain/loss is zero (namely, $\delta = 0$). Equations (3) and (5) suggest that, when $\delta = 0$, the transmission t and reflections

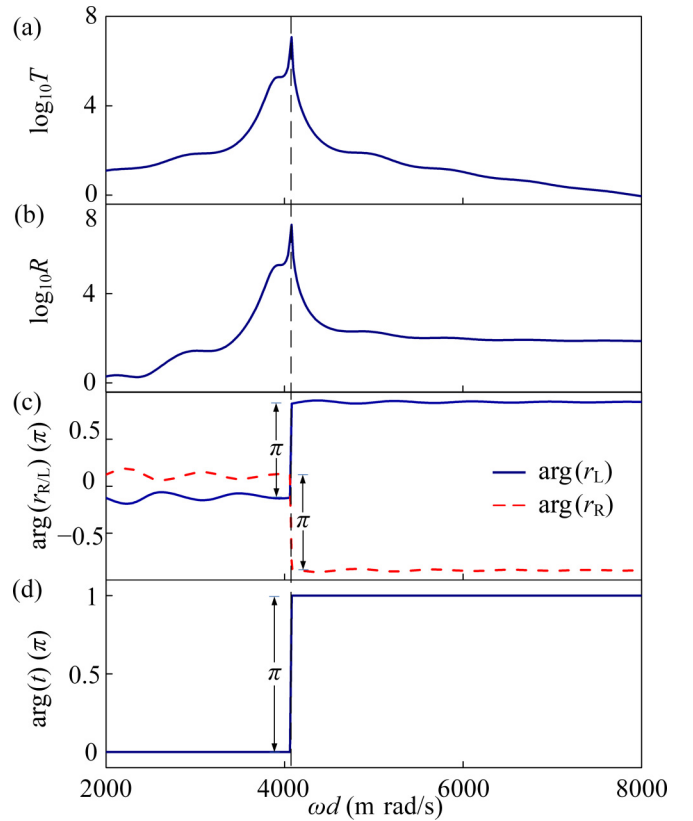


FIG. 4. Analytical results for (a) the transmittance T , (b) reflectance R , (c) phase of left/right reflection, and (d) phase of transmission versus ωd . Here, $\alpha = 1.243$ and $\delta = 0.0932$. The vertical dashed line indicates the location of $\omega d = 4080$, corresponding to a lasing mode.

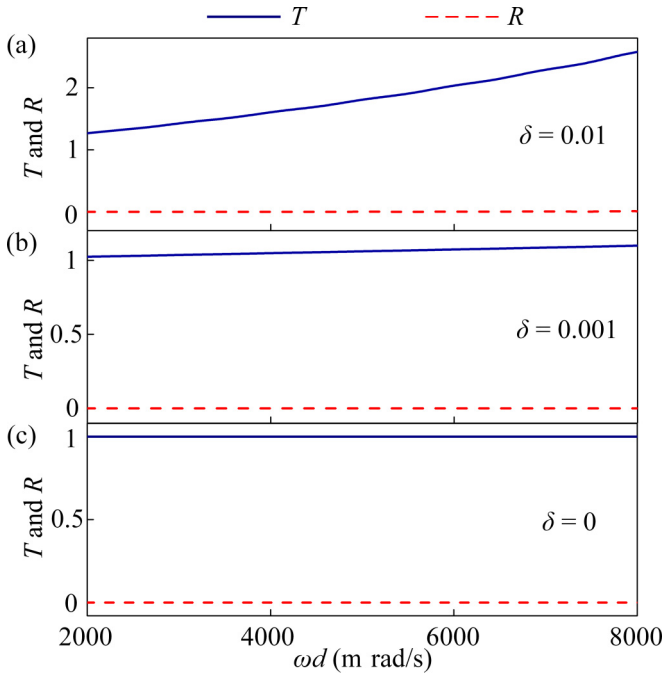


FIG. 5. Analytical results for the transmittance (blue solid line) and reflectance (red dashed line) varying with ωd for different δ . Here, $\alpha = 1.243$. In (a)–(c), $\delta = 0.01, 0.001$, and 0 , respectively.

(r_R and r_L) degrade into

$$t = 1, \quad r_L = r_R = 0, \quad (11)$$

which are independent of d and ω . Equation (11) indicates a bidirectional total transmission without any reflection, no matter what the other parameters (such as the working frequency, incident direction, and width of PIM and NIM) are. In this case, the PIM and NIM form a pair of complementary media, where they can be defined as the original medium and complementary medium (and vice versa), respectively. Acoustic wave propagation in the original and complementary medium is bilaterally symmetrical about the interface. The complementary medium can completely cancel the evolution of acoustic waves in passing through the original medium. Acoustically, the presence of the original medium is totally “canceled” by the complementary medium. The acoustic wave propagates through the structure just as if there is no PIM and NIM, so the amplitude and phase of the transmitted wave are exactly the same as those of the incident wave (namely, $t = 1$). In the ωd - δ parameter space, the case $\delta = 0$ is shown by the blue dotted line in Fig. 3(a), where it is found that the structure always works in the symmetric phase of the scattering matrix. Therefore, it is expected to be a symmetric field distribution. This bidirectional total transmission induced by the complementary medium is different from the transparency effect of \mathcal{PT} symmetric structure, where the unidirectional transparency found at the exceptional point and the bidirectional transparency induced by the Fabry-Perot resonance can only work at specific frequencies and structural parameters [5–8].

As an example, we set $\alpha = 1.243$. Figures 5(a)–5(c) plot the variation of transmittance and reflectance for $\delta = 0.01, 0.001$, and 0 , respectively. Figure 5(a) demonstrates that the

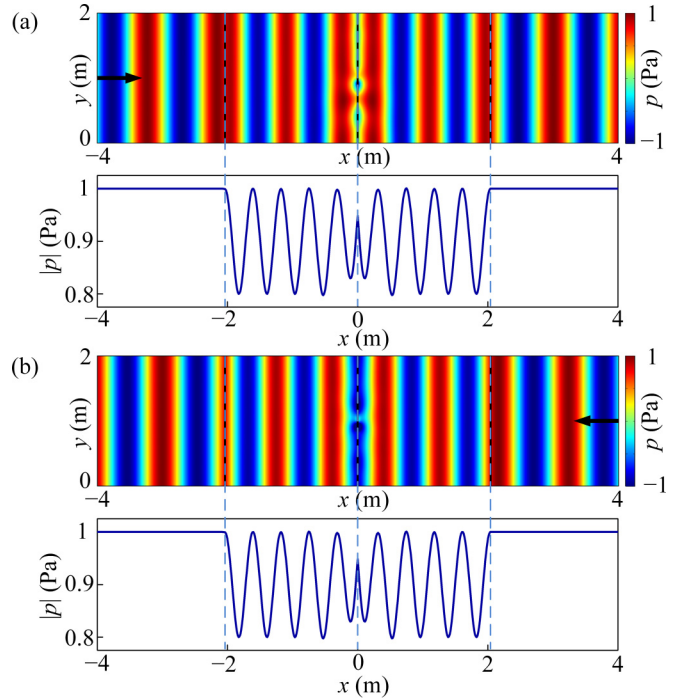


FIG. 6. Bidirectional total transmission achieved under one-port incidence. Simulated pressure field distributions (upper panels) and pressure amplitude distributions (lower panels) at the upper boundary of the A - \mathcal{PT} symmetric structure under (a) left and (b) right incidences, respectively. Here, $d = 2.04$ m, $\alpha = 1.243$, and $\delta = 0$. The amplitude and circular frequency of the incident waves are 1 Pa and $\omega = 2000$ rad/s. The vertical dashed lines indicate the boundaries between the PIM, NIM, and background medium.

transmittance and reflectance undergo a great variation with increasing ωd for $\delta = 0.01$. For $\delta = 0.001$, the variation range of transmittance decreases, as shown in Fig. 5(b). When $\delta = 0$, a unity transmittance and a zero reflectance are found in the entire frequency range, as shown in Fig. 5(c). Furthermore, we demonstrate the bidirectional total transmission with numerical simulations, as shown in Fig. 6. Here, $\alpha = 1.243$, $\delta = 0$, $d = 2.04$ m, and $\omega = 2000$ rad/s. It is found that the pressure amplitudes in the left and right background media are both 1 Pa in Figs. 6(a) and 6(b), which are equal to the incident amplitude (1 Pa). Besides, the pressure amplitude fields are symmetric to $x = 0$. The amplitude and phase of the transmitted wave are exactly the same as those of the incident wave regardless of incident direction, which verifies the effect of bidirectional total transmission.

C. Continuous coherent perfect absorption spectrum

An acoustic CPA mode occurs when two outgoing waves of the structure disappear; i.e., $A = D = 0$. Based on Eq. (2), then, the condition of achieving CPA can be concluded as

$$M_{1,1} = 0, \quad B = M_{2,1}C. \quad (12)$$

The condition $M_{1,1} = 0$ describes the structural parameters which the A - \mathcal{PT} symmetric structure should meet, and the condition $B = M_{2,1}C$ determines the amplitude and phase relationships of the two counterpropagating coherent incident

waves. The solutions of $M_{1,1} = 0$ correspond to the zeros of the scattering matrix. According to Eq. (3), $M_{1,1}$ is pure real, so $M_{1,1} = 0$ is a real function. When the parameters ωd and α are fixed, there is always a δ that satisfies $M_{1,1} = 0$. Besides, the δ solution of $M_{1,1} = 0$ is negative, indicating the required loss in the PIM/NIM. Namely, there always exists a negative δ where the A- \mathcal{PT} symmetric structure can work as a coherent perfect absorber. Therefore, the CPA mode solutions for the A- \mathcal{PT} symmetric structure are continuous in the parameter space, as shown by the black solid line in Fig. 3(a). It is found that the CPA mode takes place only in the symmetric phase of the scattering matrix. According to Eq. (4), when $M_{1,1} = 0$, we can further obtain

$$|M_{2,1}| = 1. \quad (13)$$

Equation (13) indicates that, to excite the CPA mode, the amplitudes of two coherent incidences must be equal. Besides, the required phase difference between the two coherent incidences is $\arg(M_{2,1})$, which may cover the entire range $[0, 2\pi]$.

The property of the incidences for the CPA mode achieved in A- \mathcal{PT} symmetric structure is different from that in the positive-index medium with loss [55], the zero-index medium with both gain and loss (ZIMGL) [56], and the \mathcal{PT} symmetric structure [5–8]. The systems in the first two cases are both mirror symmetric, so the CPA is obtained under two coherent incidences with equal intensity and a phase difference 0 or π . Besides, the CPA mode spectrum for the positive-index medium with loss is discrete in parameter space [55]. For the ZIMGL in Ref. [56], loss and gain are both uniformly distributed in space, but appear in different constitutive parameters of the medium. For a 1D \mathcal{PT} symmetric structure with similar arrangement, the four elementary components of the transfer matrix M' follow the properties as [5–9]

$$\text{Re}(M'_{1,2}) = \text{Re}(M'_{2,1}) = 0, \quad M'_{2,2} = M'_{1,1}. \quad (14)$$

Since $M'_{2,1}$ is pure imaginary, the relative phase difference between the two incidences for the CPA mode achieved in \mathcal{PT} symmetric structure is either $\pi/2$ or $-\pi/2$. The amplitudes of the two incidences are usually different. $M'_{1,1} = 0$ is a complex function, so the CPA mode solutions for the \mathcal{PT} symmetric structure are discrete in parameter space. Besides, the CPA mode is achieved in the symmetry-broken phase of the scattering matrix. On the contrary, the continuous CPA mode spectrum of the proposed A- \mathcal{PT} symmetric structure may facilitate the experimental realization of acoustic CPA.

We simulate an example to achieve CPA by setting $d = 2.04$ m, $\omega = 2000$ rad/s, $\alpha = 1.243$, and $\delta = -0.0932$. Therefore, the element $M_{1,1} \approx 0$, satisfying Eq. (12). Then the element $M_{2,1} = 0.9311 + 0.3665i$, so the phase angle of $M_{2,1}$ is 0.1194π . Therefore, in the simulation, two incident waves have an amplitude of 1 Pa, a circular frequency of 2000 rad/s, and a phase difference of 0.1194π , impinging on the A- \mathcal{PT} symmetric structure from the right and left, respectively. Figure 7 shows the pressure field distribution and the amplitude distribution at the upper boundary of the A- \mathcal{PT} symmetric structure. It is found that the amplitude distribution is symmetric to $x = 0$, since the system works in the symmetric phase of the scattering matrix. The pressure amplitudes in the left and right background media are both 1 Pa, which

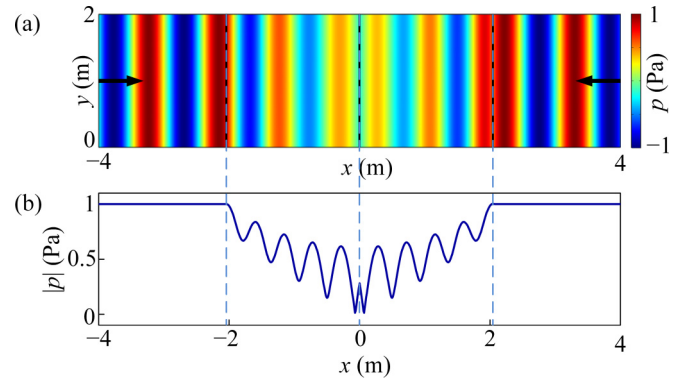


FIG. 7. Acoustic CPA achieved in the A- \mathcal{PT} symmetric structure. (a) Simulated pressure field distribution and (b) pressure amplitude distribution at the upper boundary of the A- \mathcal{PT} symmetric structure, under the incidence of two-port coherent waves with equal amplitude of 1 Pa and a phase difference of 0.1194π . Here, $d = 2.04$ m, $\alpha = 1.243$, $\delta = -0.0932$, and $\omega = 2000$ rad/s. The vertical dashed lines indicate the boundaries between the PIM, NIM, and background medium.

are equal to the amplitude of the incidence, implying that the two coherent incident waves are totally absorbed by the A- \mathcal{PT} symmetric structure without any scattering. Therefore, the A- \mathcal{PT} symmetric structure does behave as an acoustic coherent perfect absorber.

D. Continuous lasing spectrum

For a lasing mode, the boundary conditions $B = C = 0$ should be applied, so one can find the condition of achieving lasing as

$$M_{2,2} = 0. \quad (15)$$

$M_{2,2} = 0$ further leads to diverged transmittance and reflectance; i.e., $T \rightarrow \infty$ and $R \rightarrow \infty$. The solutions of $M_{2,2} = 0$ are referred to as the poles of the scattering matrix, describing the required parameters of the A- \mathcal{PT} symmetric structure. According to Eq. (3), $M_{2,2}$ is pure real, so $M_{2,2} = 0$ is a real function. Therefore, the lasing mode solutions for the A- \mathcal{PT} symmetric structure are continuous in the parameter space, as shown by the red dashed line in Fig. 3(a). The continuous CPA and lasing spectra are symmetric to $\delta = 0$, since CPA is a time-reversed counterpart of lasing. The lasing mode takes place only in the symmetric phase of the scattering matrix. When other parameters such as ωd and α of the structure are fixed, there is always a δ that satisfies $M_{2,2} = 0$. Besides, the δ solution of $M_{2,2} = 0$ is positive, indicating the required gain. Namely, there always exists a positive threshold value δ where the A- \mathcal{PT} symmetric structure can work as a laser. By inserting Eq. (15) and $B = C = 0$ into Eqs. (2) and (4), one can obtain $|M_{1,2}| = 1$ and $A = M_{1,2}D$. Therefore, the lasing mode based on the A- \mathcal{PT} symmetric structure generates two coherent outgoing waves with an equally extensive amplitude and a phase difference $\arg(M_{1,2})$. It is worth noting that the lasing mode achieved here is different from that in the \mathcal{PT} symmetric case. According to Eq. (14), $M'_{2,2} = 0$ is a complex function, so the lasing mode solutions for the \mathcal{PT} symmetric structure are discrete in the parameter space. Besides, the

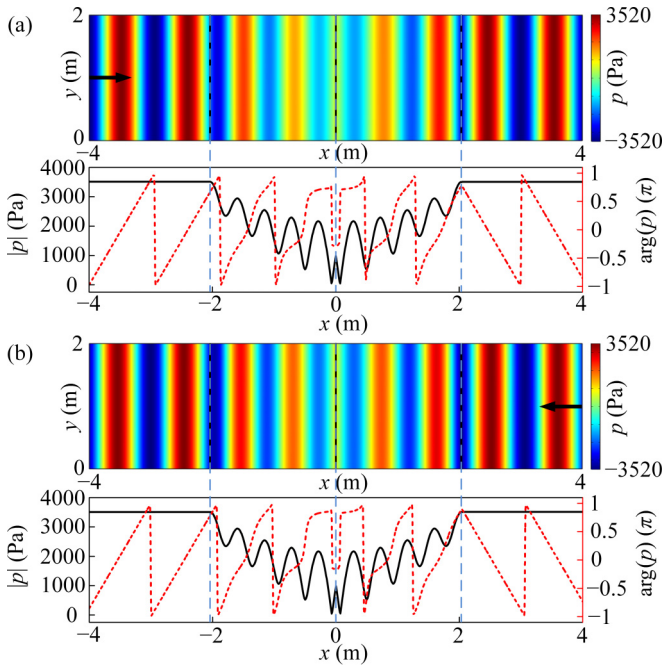


FIG. 8. Acoustic lasing achieved under one-port incidence. Simulated pressure field distributions (upper panels) and pressure amplitude/phase distributions (lower panels) at the upper boundary of the A- \mathcal{PT} symmetric structure under (a) left and (b) right incidences, respectively. In the lower panels, the black solid (red dashed) line depicts the amplitude (phase) of the pressure field. Here, $d = 2.04$ m, $\alpha = 1.243$, and $\delta = 0.0932$. The amplitude and circular frequency of the incident waves are 1 Pa and $\omega = 2000$ rad/s. The vertical dashed lines indicate the boundaries between the PIM, NIM, and background medium.

lasing mode is achieved in the symmetry-broken phase for the \mathcal{PT} symmetric structure, so the corresponding two outgoing waves usually differ in amplitude.

We show the characteristics of acoustic lasing with numerical simulations in the following. The structural parameters are set as $d = 2.04$ m, $\omega = 2000$ rad/s, $\alpha = 1.243$, and $\delta = 0.0932$, so that the element $M_{2,2} \approx 0$, satisfying Eq. (15). A plane wave with amplitude of 1 Pa is incident on the A- \mathcal{PT} symmetric structure from the left and right sides, respectively. Figures 8(a) and 8(b) show the corresponding pressure fields (upper panels) and the pressure amplitude distributions (lower panels) at the upper boundary of the structure. In both cases, the pressure amplitudes in the left and right background media are about 3520 Pa, which is much larger than the amplitude of the incident wave (1 Pa). It can be found that the amplitudes of the pressure fields are roughly symmetric to $x = 0$, but the phases of the pressure fields are not symmetric. This is because the two outgoing waves of the lasing mode have an equally extensive amplitude but a phase difference $\arg(M_{1,2})$. The quite strong fields in the background medium verify the functionality of the acoustic laser.

V. CONCLUSION

We propose an acoustic A- \mathcal{PT} symmetric structure with a pair of positive and negative index metamaterials, which

features balanced positive and negative indices, together with equal gain/loss. According to the derived scattering matrix, we observe the spontaneous phase transition for the scattering matrix, by simply modulating the frequency, local gain/loss, or geometric width. In the absence of gain/loss, the A- \mathcal{PT} symmetric structure degrades into a pair of complementary media, resulting in the bidirectional total transmission. At the zero or pole of the scattering matrix, the structure behaves as a coherent perfect absorber or a laser, respectively, which can perfectly absorb two-port coherent incident waves or radiate two coherent output waves with extensive intensity. Different from that in the \mathcal{PT} symmetric structure, these effects are all achieved in the symmetric phase, resulting in the symmetric intensity distributions. Besides, the CPA and lasing mode spectrums of the A- \mathcal{PT} symmetric structure are continuous and symmetric in the parameter space, which may facilitate the experimental realizations. The proposed A- \mathcal{PT} symmetric structure provides an alternative method to demonstrate the physics of non-Hermitian Hamiltonian, and may offer an alternative approach to design acoustic functional devices such as absorber, sensors, and amplifiers.

ACKNOWLEDGMENT

This work was supported by the National Natural Science Foundation of China (Grants No. 12027808, No. 11874222, No. 12174197, and No. 11704192).

APPENDIX A: DERIVATION OF TRANSFER MATRIX M

For linear and harmonic acoustic waves propagating in a 1D structure, where all field quantities have a time variation $e^{-i\omega t}$ with ω being the angular frequency, the spatial distribution of sound pressure $p(x)$ satisfies the 1D acoustic wave equation

$$\frac{d^2 p(x)}{dx^2} + \left(\frac{\omega}{c_0}\right)^2 n^2(x)p(x) = 0. \quad (\text{A1})$$

Here, c_0 is the acoustic velocity of the background medium, and $n(x)$ is the acoustic refractive index.

Consider a 1D acoustic multilayered structure consisting of N layers of media, which is immersed in a background medium with a density of ρ_0 and a velocity of c_0 . The thickness, density, and refractive index of the j th layer are $d_j = x_j - x_{j-1}$, ρ_j , and n_j , respectively, where x_{j-1} and x_j denote the coordinates of the left and right boundaries of the j th layer. All these media are homogeneous and isotropic. Among them, the 0th and $(N + 1)$ -th layers are left and right background media.

The total field within each medium could be regarded as a superposition of forward and backward propagating waves. Therefore, the pressure field (p) within the j th layer can be expressed as

$$p_j(x) = a_j e^{ik_j(x-x_j)} + b_j e^{-ik_j(x-x_j)}, \quad (\text{A2})$$

where k_j is the wave number for the j th layer; a_j and b_j are the amplitudes of the backward and forward propagating wave components, respectively. The scattering model of this multilayered structure could be similarly arranged as Fig. 1. Particularly, the pressure field in the background medium is

expressed as

$$\begin{aligned} p_0(x) &= A e^{ik_0(x-x_0)} + B e^{-ik_0(x-x_0)}, \quad x < x_0, \\ p_{N+1}(x) &= C e^{ik_0(x-x_N)} + D e^{-ik_0(x-x_N)}, \quad x > x_N, \end{aligned} \quad (\text{A3})$$

Here, k_0 is the wave number for the background medium, A and B are the amplitudes of the backward and forward propagating waves within the left background medium, and C and D are the amplitudes of the backward and forward propagating waves within the right background medium, respectively. Accordingly, the normal velocity field (v) in each medium can be expressed as

$$v_j(x) = \frac{i}{\omega \rho_j} \frac{\partial p_j(x)}{\partial x}. \quad (\text{A4})$$

The continuous conditions of acoustic pressure and normal velocity fields at the interface x_j lead to

$$\begin{aligned} p_j(x_j) &= p_{j+1}(x_j), \\ v_j(x_j) &= v_{j+1}(x_j). \end{aligned} \quad (\text{A5})$$

By inserting Eqs. (A2) and (A4) into Eq. (A5), one can obtain

$$\begin{bmatrix} a_j \\ b_j \end{bmatrix} = M_j \begin{bmatrix} a_{j+1} \\ b_{j+1} \end{bmatrix}, \quad (\text{A6})$$

where

$$M_j = \frac{1}{2} \begin{bmatrix} 1 + \frac{Z_j}{Z_{j+1}} & 1 - \frac{Z_j}{Z_{j+1}} \\ 1 - \frac{Z_j}{Z_{j+1}} & 1 + \frac{Z_j}{Z_{j+1}} \end{bmatrix} \begin{bmatrix} e^{-ik_{j+1}d_{j+1}} & 0 \\ 0 & e^{ik_{j+1}d_{j+1}} \end{bmatrix}. \quad (\text{A7})$$

Here, $Z_j = \frac{\rho_j c_0}{n_j}$ is the acoustic impedance for the j th layer medium. By straightly iterating Eqs. (A6) and (A7), the acoustic fields in the left and right background media can be related by

$$\begin{bmatrix} A \\ B \end{bmatrix} = M \begin{bmatrix} C \\ D \end{bmatrix}, \quad (\text{A8})$$

where the transfer matrix $M = \begin{bmatrix} M_{1,1} & M_{1,2} \\ M_{2,1} & M_{2,2} \end{bmatrix}$ finally reads

$$M = \frac{1}{2} \left(\prod_{j=0}^{N-1} M_j \right) \begin{bmatrix} 1 + \frac{Z_N}{Z_{N+1}} & 1 - \frac{Z_N}{Z_{N+1}} \\ 1 - \frac{Z_N}{Z_{N+1}} & 1 + \frac{Z_N}{Z_{N+1}} \end{bmatrix}. \quad (\text{A9})$$

Equation (A9) describes the transfer matrix M for a general multilayered structure, and the transmission and reflection coefficients of the structure can be further expressed in terms of the components of M . The transfer matrix method could also deal with an inhomogeneous medium, since an inhomogeneous medium can be approximated with multilayered homogeneous media.

As for the proposed A- \mathcal{PT} symmetric structure shown in Fig. 1, $N = 2$, $\rho_1 = \rho_0$, $\rho_2 = -\rho_0$, $n_1 = \alpha + i\delta$, $n_2 = -\alpha + i\delta$, and $d_1 = d_2 = d$. By inserting these parameters into Eq. (A9), one can obtain

$$\begin{aligned} M &= \frac{1}{8} \begin{bmatrix} 1 + \frac{Z_0}{Z_1} & 1 - \frac{Z_0}{Z_1} \\ 1 - \frac{Z_0}{Z_1} & 1 + \frac{Z_0}{Z_1} \end{bmatrix} \begin{bmatrix} e^{-ik_1 d} & 0 \\ 0 & e^{ik_1 d} \end{bmatrix} \begin{bmatrix} 1 + \frac{Z_1}{Z_2} & 1 - \frac{Z_1}{Z_2} \\ 1 - \frac{Z_1}{Z_2} & 1 + \frac{Z_1}{Z_2} \end{bmatrix} \\ &\times \begin{bmatrix} e^{-ik_2 d} & 0 \\ 0 & e^{ik_2 d} \end{bmatrix} \begin{bmatrix} 1 + \frac{Z_2}{Z_0} & 1 - \frac{Z_2}{Z_0} \\ 1 - \frac{Z_2}{Z_0} & 1 + \frac{Z_2}{Z_0} \end{bmatrix}. \end{aligned} \quad (\text{A10})$$

Here, $k_1 = (\alpha + i\delta)k_0$, $k_2 = (-\alpha + i\delta)k_0$, $Z_0 = \rho_0 c_0$, $Z_1 = \frac{Z_0}{\alpha + i\delta}$, and $Z_2 = \frac{Z_0}{\alpha - i\delta}$. Simplifying Eq. (A10) leads to the explicit expression of M , as shown by Eq. (3).

APPENDIX B: DERIVATION OF EQ. (6)

Consider a 1D general acoustic A- \mathcal{PT} symmetric structure, consisting of N layers of homogeneous and isotropic media, immersed in a background medium with density ρ_0 and velocity c_0 . The complex refractive index profile of the A- \mathcal{PT} symmetric structure could be arbitrary but satisfies $n(x) = -n^*(-x)$. The density of the A- \mathcal{PT} symmetric structure is real and satisfies $\rho(x) = -\rho(-x)$. With a similar arrangement as Fig. 1, the transfer matrix M (at a real angular frequency ω) of the general A- \mathcal{PT} symmetric structure could be obtained as Eq. (A9).

Now we carry out an operation,

$$\rho_j \rightarrow -\rho_j, \quad n_j \rightarrow -n_j^*. \quad (\text{B1})$$

Namely, we flip the sign of the density and replace the refractive index into its negative complex conjugate for each layer (labeled j) of the general A- \mathcal{PT} symmetric structure. Then, the original transfer matrix M becomes its complex conjugate, namely,

$$M \rightarrow M^*. \quad (\text{B2})$$

This is because, under the operation of Eq. (B1), all the matrix M_j [Eq. (A7)] and acoustic impedance Z_j , which are used to derive M as shown by Eq. (A9), become their corresponding complex conjugates. Since the transmission and reflection coefficients are expressed in terms of the components of M , as shown by Eq. (5), these coefficients also become their corresponding complex conjugates under the operation of Eq. (B1), namely,

$$t_L \rightarrow t_L^*, \quad t_R \rightarrow t_R^*, \quad r_L \rightarrow r_L^*, \quad r_R \rightarrow r_R^*. \quad (\text{B3})$$

It is noted that for the 1D A- \mathcal{PT} symmetric structure satisfying $n(x) = -n^*(-x)$ and $\rho(x) = -\rho(-x)$, the operation of Eq. (B1) is equivalent to flipping the structure in the left-right direction. Therefore, this operation also leads to

$$t_L \rightarrow t_R, \quad t_R \rightarrow t_L, \quad r_L \rightarrow r_R, \quad r_R \rightarrow r_L. \quad (\text{B4})$$

Comparing Eqs. (B3) and (B4), one can find

$$t_L = t_R^*, \quad r_L = r_R^*. \quad (\text{B5})$$

Equation (B5) and $t = t_L = t_R$, guaranteed by acoustic reciprocity, finally lead to $\text{Im}(t) = 0$ and $r_L = r_R^*$, as shown by Eq. (6).

- [1] C. M. Bender and S. Boettcher, *Phys. Rev. Lett.* **80**, 5243 (1998).
- [2] C. E. Rüter, K. G. Makris, R. El-Ganainy, D. N. Christodoulides, M. Segev, and D. Kip, *Nat. Phys.* **6**, 192 (2010).
- [3] K. G. Makris, R. El-Ganainy, D. N. Christodoulides, and Z. H. Musslimani, *Phys. Rev. Lett.* **100**, 103904 (2008).
- [4] P. A. Brandão and S. B. Cavalcanti, *Phys. Rev. A* **96**, 053841 (2017).
- [5] S. Longhi, *Phys. Rev. A* **82**, 031801(R) (2010).
- [6] Y. D. Chong, L. Ge, and A. D. Stone, *Phys. Rev. Lett.* **106**, 093902 (2011).
- [7] W.-Q. Ji, Q. Wei, X.-F. Zhu, D.-J. Wu, and X.-J. Liu, *Europhys. Lett.* **125**, 58002 (2019).
- [8] Y. Y. Fu, Y. D. Xu, and H. Y. Chen, *Opt. Express* **24**, 1648 (2016).
- [9] L. Ge, Y. D. Chong, and A. D. Stone, *Phys. Rev. A* **85**, 023802 (2012).
- [10] Z. P. Gong, Y. Ashida, K. Kawabata, K. Takasan, S. Higashikawa, and M. Ueda, *Phys. Rev. X* **8**, 031079 (2018).
- [11] X. F. Zhu, H. Ramezani, C. Z. Shi, J. Zhu, and X. Zhang, *Phys. Rev. X* **4**, 031042 (2014).
- [12] R. Fleury, D. Sounas, and A. Alù, *Nat. Commun.* **6**, 5905 (2015).
- [13] A. V. Poshakinskiy, A. N. Poddubny, and A. Fainstein, *Phys. Rev. Lett.* **117**, 224302 (2016).
- [14] A. Guo, G. J. Salamo, D. Duchesne, R. Morandotti, M. Volatier-Ravat, V. Aimez, G. A. Siviloglou, and D. N. Christodoulides, *Phys. Rev. Lett.* **103**, 093902 (2009).
- [15] L. Feng, M. Ayache, J. Q. Huang, Y.-L. Xu, M.-H. Lu, Y.-F. Chen, Y. Fainman, and A. Scherer, *Science* **333**, 729 (2011).
- [16] S. Weimann, M. Kremer, Y. Plotnik, Y. Lumer, S. Nolte, K. G. Makris, M. Segev, M. C. Rechtsman, and A. Szameit, *Nat. Mater.* **16**, 433 (2017).
- [17] T. Liu, X. Zhu, F. Chen, S. Liang, and J. Zhu, *Phys. Rev. Lett.* **120**, 124502 (2018).
- [18] R. El-Ganainy, K. G. Makris, M. Khajavikhan, Z. H. Musslimani, S. Rotter, and D. N. Christodoulides, *Nat. Phys.* **14**, 11 (2018).
- [19] L. Ge and H. E. Türeci, *Phys. Rev. A* **88**, 053810 (2013).
- [20] J.-H. Wu, M. Artoni, and G. C. La Rocca, *Phys. Rev. Lett.* **113**, 123004 (2014).
- [21] P. Peng, W. X. Cao, C. Shen, W. Z. Qu, J. M. Wen, L. Jiang, and Y. H. Xiao, *Nat. Phys.* **12**, 1139 (2016).
- [22] D. A. Antonosyan, A. S. Solntsev, and A. A. Sukhorukov, *Opt. Lett.* **40**, 4575 (2015).
- [23] F. Yang, Y.-C. Liu, and L. You, *Phys. Rev. A* **96**, 053845 (2017).
- [24] X.-L. Zhang, T. Jiang, and C. T. Chan, *Light Sci. Appl.* **8**, 88 (2019).
- [25] S. L. Ke, D. Zhao, J. X. Liu, Q. J. Liu, Q. Liao, B. Wang, and P. X. Lu, *Opt. Express* **27**, 13858 (2019).
- [26] Y. Choi, C. Hahn, J. W. Yoon, and S. H. Song, *Nat. Commun.* **9**, 2182 (2018).
- [27] Y. Li, Y.-G. Peng, L. Han, M.-A. Miri, W. Li, M. Xiao, X.-F. Zhu, J. Zhao, A. Alù, S. Fan, and C.-W. Qiu, *Science* **364**, 170 (2019).
- [28] V. V. Konotop and D. A. Zezyulin, *Phys. Rev. Lett.* **120**, 123902 (2018).
- [29] Z. Y. Liu, X. Zhang, Y. Mao, Y. Y. Zhu, Z. Yang, C. T. Chan, and P. Sheng, *Science* **289**, 1734 (2000).
- [30] Y. Ding, Z. Liu, C. Qiu, and J. Shi, *Phys. Rev. Lett.* **99**, 093904 (2007).
- [31] G. Ma and P. Sheng, *Sci. Adv.* **2**, e1501595 (2016).
- [32] M. Landi, J. J. Zhao, W. E. Prather, Y. Wu, and L. K. Zhang, *Phys. Rev. Lett.* **120**, 114301 (2018).
- [33] B. Assouar, B. Liang, Y. Wu, Y. Li, J. C. Cheng, and Y. Jing, *Nat. Rev. Mater.* **3**, 460 (2018).
- [34] H. Y. Chen and C. T. Chan, *J. Phys. D: Appl. Phys.* **43**, 113001 (2010).
- [35] S. A. Cummer and D. Schurig, *New J. Phys.* **9**, 45 (2007).
- [36] S. Zhang, C. Xia, and N. Fang, *Phys. Rev. Lett.* **106**, 024301 (2011).
- [37] N. Fang, D. Xi, J. Xu, M. Ambati, W. Srituravanich, C. Sun, and X. Zhang, *Nat. Mater.* **5**, 452 (2006).
- [38] B. Liang, X. S. Guo, J. Tu, D. Zhang, and J. C. Cheng, *Nat. Mater.* **9**, 989 (2010).
- [39] N. Boechler, G. Theocharis, and C. Daraio, *Nat. Mater.* **10**, 665 (2011).
- [40] J. Zhu, J. Christensen, J. Jung, L. Martin-Moreno, X. Yin, L. Fok, X. Zhang, and F. J. Garcia-Vidal, *Nat. Phys.* **7**, 52 (2011).
- [41] Y. Cheng, C. Zhou, B. G. Yuan, D. J. Wu, Q. Wei, and X. J. Liu, *Nat. Mater.* **14**, 1013 (2015).
- [42] C. Xu, G. Ma, Z.-G. Chen, J. Luo, J. Shi, Y. Lai, and Y. Wu, *Phys. Rev. Lett.* **124**, 074501 (2020).
- [43] H. He, C. Qiu, L. Ye, X. Cai, X. Fan, M. Ke, F. Zhang, and Z. Liu, *Nature (London)* **560**, 61 (2018).
- [44] Z. Liang and J. Li, *Phys. Rev. Lett.* **108**, 114301 (2012).
- [45] Y. Li, C. Shen, Y. Xie, J. Li, W. Wang, S. A. Cummer, and Y. Jing, *Phys. Rev. Lett.* **119**, 035501 (2017).
- [46] L. Fan and J. Mei, *Phys. Rev. Appl.* **14**, 044003 (2020).
- [47] Z. Zhang, M. Rosendo López, Y. Cheng, X. Liu, and J. Christensen, *Phys. Rev. Lett.* **122**, 195501 (2019).
- [48] Y. Cheng, J. Y. Xu, and X. J. Liu, *Phys. Rev. B* **77**, 045134 (2008).
- [49] L. Chen, L. Fan, and S. Y. Zhang, *Phys. Rev. B* **100**, 024111 (2019).
- [50] Y. Lai, H. Y. Chen, Z.-Q. Zhang, and C. T. Chan, *Phys. Rev. Lett.* **102**, 093901 (2009).
- [51] H. M. Nguyen, *Adv. Nonlinear Anal.* **7**, 449 (2018).
- [52] A. Mostafazadeh, *Phys. Rev. A* **80**, 032711 (2009).
- [53] K. Kawabata and S. Ryu, *Phys. Rev. Lett.* **126**, 166801 (2021).
- [54] C. Rasmussen, L. Quan, and A. Alù, *J. Appl. Phys.* **129**, 210903 (2021).
- [55] Y. D. Chong, L. Ge, H. Cao, and A. D. Stone, *Phys. Rev. Lett.* **105**, 053901 (2010).
- [56] P. Bai, K. Ding, G. Wang, J. Luo, Z.-Q. Zhang, C. T. Chan, Y. Wu, and Y. Lai, *Phys. Rev. A* **94**, 063841 (2016).